Water Turbidity Monitoring using Satellite Imagery in New Zealand Waterways

Forest Engineering Honours Project

September 2021

Liam Gilroy
University of Canterbury

Acknowledgments

This dissertation was only made possible through the actions and support of many other people. Firstly, thank you to Professor Rien Visser, my supervisor and guidance throughout this project. Thank you to the Waikato Regional Council and Environment Canterbury for the access to their datasets, without which this would not have been possible. Thank you to my colleagues, lecturers, and people I've had contact with within the industry, all of whom have provided valuable feedback and insight into the project. Finally, thank you to my family whose love and support made this entire journey possible.

Without this help, I sincerely doubt I would be where I am today.

Abstract

Waterways, water, and aquatic ecosystems must be safeguarded. For forestry and forest practices, both the RMA and ECOP recognise the importance of protecting and monitoring water quality. Turbidity is a qualitative measure of the amount of sediment in a waterway and a key indicative measure of water quality. The in-situ monitoring of turbidity in narrow waterways is both expensive and difficult. The opportunity to get indirect values using large spatial resolution datasets is not plausible with current technology. This report assesses the potential of using satellite imagery to estimate turbidity of waterways within New Zealand.

Estimations of turbidity were made from satellite imagery (PlanetScope) using the semi-empirical, generic equation developed by Nechad. This equation is unique in that it allows for the estimation of turbidity without prior derivation of a reflectance and turbidity relationship, requiring in-situ, site-specific measurements. 141 estimations of turbidity across four sites were made and compared to continuous in-situ data to assess the potential of the technology. There were two sites each in the Waikato River and Heathcote Stream respectively, each with varying widths and site conditions. The four bands of the PlanetScope satellite imagery were compared for the accuracy of estimated turbidites.

Results showed the green band (500-590Nm) produced the most accurate estimations of turbidity, followed by the red band (590-670Nm). Turbidity estimations could be made at three of the four sites. The final site could not be used as the river width and vegetation cover meant appropriate sampling locations could not be determined. The method identified changes and peaks in turbidity, providing appropriate satellite imagery was available. However, the accuracy of the estimations was not ideal, with the highest R^2 value of 0.26. It also tended to overestimate turbidity, with an average bias of 4.32 FNU. This is likely due to the calibration of Nechad's equation that was developed for moderately turbid, coastal waters. Thus, the method is likely to have the most efficient application when used in conjunction with in-situ testing, identifying areas of high turbidity or points of change and allowing for further monitoring to be completed. Other key limitations of the method include the waterway width, imagery availability, and weather conditions (cloud cover).

In summary, there exists large potential in the application of remote sensing in the turbidity estimation and monitoring of waterways. This would be especially true if the research was undertaken for the recalibration of Nechad's equation for inland, freshwater waterways. This would allow the development of a high spatial and temporal resolution dataset at a lower cost compared to other monitoring methods.

Table of Contents

1. Introduction

Turbidity is a qualitative measure of the amount of suspended sediment particles in water and a key indicator of water quality. Turbidity is strongly correlated with sediment, nutrients, and bacteria within water and has been used as a surrogate measurement for the impact of humans on waterways, monitoring of sediment levels and natural streams below soil moving operations (Sadar, 2017).

Turbidity is measured as the relative clarity of water, in which the presence of suspended sediment particles block and scatter light transmittance (attenuation). High visual clarity of water better meets the recreational and aesthetic values often desired by users. As the turbidity value increases, the amount of suspended sediment particles within the water is also likely to increase (Sadar, 2017). High levels of suspended sediment can have adverse effects on aquatic life, the most significant caused by light attenuation. This is due to the reduced vision of sighted aquatic organisms and reduced penetration of light for photosynthesis. Increased suspended sediment can also directly cause benthic smothering and irritation of fish gills (Davies-Colley & Smith, 2001). However, it should be noted that although increased levels of suspended sediment particles can cause these detrimental environmental effects, these do not always occur. Thus, it is not a direct measure of environmental health.

Water quality is recognised as a key environmental factor that must be protected by the RMA (Resource Management Act 1991) (Reddy, 2017) and ECOP (Environmental Code of Practice for Plantation Forest) (NZFOA, 2015), both of which are governing documents for forestry operations within New Zealand. Turbidity as an indicative measure of water quality is often used for identifying possible detrimental effects that these operations can have on waterways. However, the continual in-situ monitoring of turbidity using field turbidity monitors is difficult, expensive and cannot be completed retrospectively. Monthly monitoring or similar regimes can also be expensive or difficult due to limited access and associated time requirements. It has the potential to miss key sedimentation events.

The National River Water Quality Network (NRWQN) is the most comprehensive freshwater quality monitoring network in New Zealand, consisting of 77 sites on 35 rivers (NIWA, 2020). Turbidity is measured in the NRWQN using handheld turbidity sensors in either FNU (Formazin Nephelometric Units) or NTU (nephelometric turbidity units), dependant on equipment availability. Secchi depth is also commonly used in New Zealand for measuring water clarity (higher turbidity reduces clarity) (Hamill & Lew, 2006). Secchi depth is like black disc depth but uses a black and white disk measured vertically, rather than the horizontal measurement of the black disc. However, both measurements have been replaced in the National Policy Statement for freshwater Management by the Visual Water Clarity Tube measurement. Thus, there is no standardised testing equipment or measurement units across New Zealand.

Turbidity measurements are qualitative rather than quantitative, or that turbidity units such as NTU (Nephelometric Turbidity Units) and FNU have “no intrinsic physical, chemical or biological significance” (Campbell Scientific, 2014). Thus, conversions between units or TSS (total suspended solids) are not possible; relationships can be derived although they will only hold true for a unique condition set. Particle size, type and distribution will all change these conditions meaning a new model must be developed for each site, at each point in time

(Fondriest, 2014). Below, Figure 1 shows the relative clarity of water samples at a range of turbidity (NTU) levels.

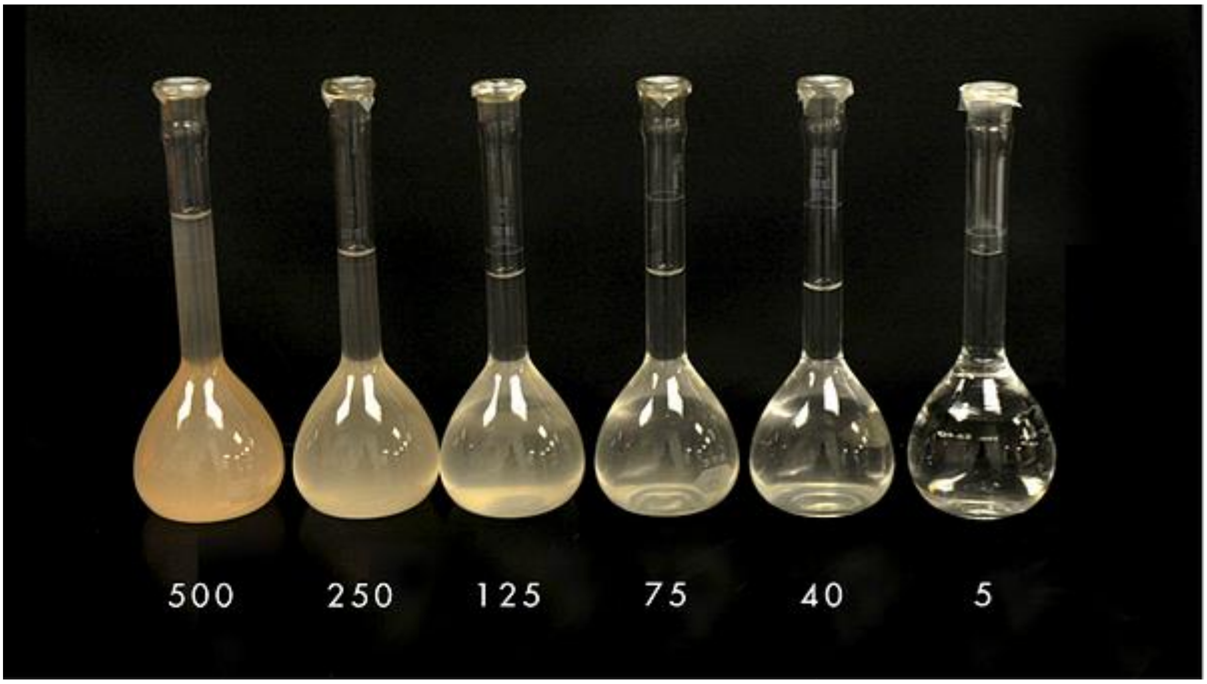

Figure 1 – *Relative clarity of water samples at a range of turbidities (NTU) (SABD, 2018)*

This study aims to assess the potential of using remote sensing to determine the turbidity of waterways within New Zealand. Through the use of satellite imagery with fine spatial resolution and the spectral responses of individual pixels within waterways, it is hoped a turbidity value can be estimated. This will be achieved through analysis of suitable satellite imagery using the generic, multisensory equation developed by Nechad et al. (2010) for the determination of turbidity in moderately turbid waters. The estimated value will then be compared to synchronous in-situ measurements taken from continuous turbidity datasets provided by the Waikato Regional Council and Environment Canterbury.

The results will be useful for helping determine historic turbidity levels and act as a substitution for, or assisting with, in-situ testing. As satellite data is temporal and archived, this could allow for the historic turbidity of a site to be determined without any testing data equipment previously being installed, assuming archived imagery is available (n.b. archive imagery is data more than 90 days old for PlanetScope constellations). This has a large range of potential applications including judicial decisions, quantification of effects on water quality and establishing long term benchmarks. It could also be used for monitoring a waterway along its length, allowing for the determination of point sources of pollution.

2. Literature Review

2.1 – Turbidity in Forestry

The impact of forestry on water quality is recognised as a critical component of forestry management (Tobin et al., 2007). Turbidity is an indicative measure of water quality and thus, the management of it is also a critical component of forestry management. The major causes of increased sediment levels (and thereby turbidity) in waterways due to forestry, is caused by the soil disturbance associated with activities such as cultivation, drainage, road construction and harvesting (Nisbet, 2001). Governing documents such as the ECOP, RMA and other countries' forest and water quality guidelines are intended to reduce the possible negative effects that forestry and other activities have on water quality.

Webb and Haywood (2005) show forestry activities can provide both point and non-point sources of pollution. Point sources consist of forded river crossings, direct drainage discharge into a stream, or a slip event. Non-point sources may be caused by reduced groundcover conditions, soil compaction, and soil disturbance. These cause increased level of soil erosion resulting in increased suspended sediment concentrations. They further note that without soil conservation measures, "turbidities in excess of 100 NTU would not be unexpected during forestry operations" and in more extreme cases "it is conceivable that localised stream turbidity during an intense rainstorm could exceed 1000 NTU". This represents severe negative repercussions both environmentally and for the suitability of water downstream for other use cases such as drinking or agriculture. Therefore, qualitative measurements such as turbidity are crucial indicators of forestry's performance in protecting water quality.

2.2 - Coarse Spatial Resolution Applications

The turbidity of large waterbodies such as oceans and large lakes, have been measured remotely since 1974 when the first ocean observing satellites were launched. These used polychromatic imagery to detect water colour, which after a relationship with in-situ turbidity measurements was formed, allowed for the estimation of turbidity. The first relationship of estimated turbidity and suspended sediment concentrations was developed in 1981 (Curran & Novo, 1988). These results tended to be inaccurate and inconsistent, with typical r^2 values of around 0.5.

Following the launch of multiple ocean colour satellites clusters after 2002 (e.g. Aqua by NASA) much progress was made in determining turbidity and other indicative measures of water quality (Shen et al., 2014). These satellites differ from traditional polychromatic imagery as they achieve much greater accuracies when measuring light radiance, reflectance, and backscatter. This allows for much more precise measurements of light attenuation and thereby derivation of turbidity. Using ocean colour satellite clusters, Binding et al. (2005) achieved errors of 12% in moderately turbid coastal waters when estimating turbidity. Further refinement of techniques and a better understanding of atmospheric interference allowed Chen et al. (2007) to achieve r^2 values of 0.97 in low turbidity waters. However, the low spatial resolutions of ocean colour sensors make them unsuitable for coastal and smaller water bodies. The resolutions of these sensors range from 200m to 4km, with the majority being around 350m (Groom et al., 2019).

As satellite sensor capability increased with time, spatial resolution become finer, leading to the launch of satellites such as Landsat-8 (2013, 30 m) and Sentinel-2 (2015, 20 m). These finer resolutions allowed for measurements of smaller waterbodies and coastal or estuarine environments. Kuhn et al. (2019) compared synchronous imagery in large rivers to over 6000 in-situ measurements taken by boat, recording mean errors of 4% and 13% between estimated and in-situ measurements for the Landsat and Sentinel clusters, respectively. Larger errors were observed in higher turbidity waters, and both clusters tended to overestimate; this was attributed to the additional contributions to the red band from surface glint. Inconsistencies in radiometric calibration between different sensors were estimated to account for 6% of the observed error. Pereira et al. (2018) achieved r^2 values of 0.88 between estimated and in-situ turbidity values using the Landsat-8 cluster in the Mississippi River basin. This was achieved across a turbidity range of 80 to 2200 FNU, or suspended sediment concentrations from 44 to 1130 mg/L, with estimated turbidity values below 300 FNU tending to be more accurate. Pereira et al. (2018) further acknowledged the use of remote sensing in addressing temporal gaps in datasets and the measurement of turbidity where no in-situ measurements are available.

2.3 - Fine Spatial Resolution Applications

Further development in sensor capabilities has again reduced spatial resolutions, with clusters now achieving <10 m resolutions. This creates the possibility of measuring the turbidity of much narrower waterways. Other sensor developments include an increase in the range of spectral reflectance measured. An example of this is the red-edge band of the now-retired RapidEye cluster; this is described in a white paper by RapidEye (2012) as the transition between red and NIR (Near-Infra-Red) bands (690-730 nm). It is useful for estimating Secchi depth; initial studies showed RMSE (Root Mean Square Error) of <0.7 m between estimated Secchi depth and recorded depth in estuaries with average Secchi depths ranging from to 1-10 m (Gallegos et al., 1990). Thus, the red-edge band has been used to great effect for water quality monitoring (RapidEye, 2012).

Yigit Avdan et al. (2019) applied the red-edge band and RapidEye data to a smaller lake during a study in which multiple control points were selected and then compared to the estimated turbidity using a variety of different turbidity indices. The highest correlation of different reflectance bands occurred between the in-situ turbidity and red-edge band with an R-value of 0.9. Note that the spatial resolution of the data at this location was 5m, while the average spatial resolution of the RapidEye data is 6.5m worldwide. Vanhellemont (2019) also investigated water quality parameters using both RapidEye and PlanetScope satellite data (0.5 m spatial resolution). They stated, “with their high ground resolution [in reference to RapidEye], these satellites could provide turbidity estimates in highly productive waters, smaller lakes and ponds, or narrow rivers.” Their results showed an RMSE value of 6 FNU for water quality monitoring in moderately turbid (<80 FNU) coastal and inland waters.

Yigit Avdan et al. (2019) and Vanhellemont (2019) both measured waterways in which multiple adjacent pixels fit within the waterways, averaging the estimations. Isidro et al. (2018) investigated the use of only a single pixel that fit completely within the riverbanks, analysing quantifying the sediment levels in small rivers (4-10m width) using RapidEye (6.5m), Plediade-1A (2m) and Spot6 (6m) satellite imagery. Key findings showed that as waterway width increased, the standard deviation in measurements decreased, although results could still be obtained from smaller waterways. Issues faced include very low water levels (150 to 350mm), protruding rocks distorting results, and high turbidity levels. Note that a key difference between Isidro et al. (2018) and my proposal is Isidro quantitively measures suspended sediment concentration, while I propose to measure turbidity (qualitative).

The results of Yigit Avdan et al. (2019), Vanhellemont (2019) and Isidro et al. (2018) are meaningful for my proposal. Each was able to estimate turbidity or suspended sediment concentrations in much smaller waterways than previously achievable with older satellite technology. Both Yigit and Vanhellemont achieved high levels of accuracies in large waterways, while Isidro achieved lower levels of accuracies in a highly difficult waterway. There is a gap in research literature for the possibility of using remote sensing in narrow waterways to estimate turbidity.

McCabe et al. (2017) stated that the PlanetScope (Cubesat) satellites with their unprecedented temporal and spatial resolutions could be used as an alternative method for assessing water quality using photogrammetry. However, Topp et al. (2020) found they were prone to geolocation accuracy errors, radiometric inconsistencies across satellites and required difficult atmospheric corrections. Vanhellemont (2019) quantified the radiometric inconsistencies between near-simultaneous PlanetScope images as 10% within the red band, and around 40% for the NIR band. Thus, the PlanetScope imagery has a lot of potential but would require a large amount of testing regarding image classification and quality control to produce accurate and consistent results. The Hyperion satellite cluster (2.5m spatial resolution) also showed initial promise for inland water quality measurements but suffers from radiometric instability and high noise to signal ratio (Topp et al., 2020).

Seeqeunt is currently developing a satellite-based water quality monitoring system that could monitor the quality of every lake globally and is being tested and funded within New Zealand (Seequent, 2019). This utilises the Trophic Level Index, calculating nitrogen, phosphorus, clarity (turbidity), and chlorophyll-a. The project aims to autonomously monitor the health of all New Zealand's lakes and use historical data to identify seasonal trends. A trial showed promising trends between estimated and measured variables for two lakes in the Canterbury region (Seequent, 2020). This relies on the older Landsat-8 satellites with coarser spatial resolutions (30m) but highlights the possibility of autonomous monitoring systems for waterways.

3. Objectives

This study aims to assess the potential of using satellite imagery to determine the turbidity of waterways within New Zealand.

This could allow for the determination of current and historic turbidity levels of waterways, identification of point sources of pollution and enable further research into large scale monitoring of waterways for water quality purposes at previously impractical data resolutions.

4. Methodology

4.1 - Data Collection

For this study, in-situ turbidity measurements were used to assess the accuracy of estimated measurements from satellite data, thus the limited availability of continuous in-situ data determined the sites that could be used. Data was kindly provided by the Waikato Regional Council for the Waikato River, and by Environment Canterbury for the Heathcote stream. This data consists of continuous turbidity measurements from in-situ instruments over the previous years. The four data collection sites are described in Table 2.

Table 1 - *Description and location of site data with continuous turbidity data logging.*

Site	General Description	Width (m)	Coordinates
A	Waikato river elbow near outlet, wide, rural	250	-37.283, 174.843
B	Waikato river elbow in Hamilton, city	60	-37.791, 175.290
C	Heathcote Stream, tree cover present	8	-43.572, 172.617
D	Heathcote Stream, urban, narrow	6	-43.560, 172.648

The sensor data was then checked over for issues, for example, Site C has patchy data during low flow periods and Site D initially suffered from power consumption and lens issues. Thus, suitable periods of data were selected; these are periods of relatively consistent readings with gradual changes in turbidity over time and no quality issues noted by the operating technician. The turbidity readings for each day from 9am to 1pm were averaged, with the mean turbidity value used as the baseline for gauging the accuracy of the satellite estimations of turbidity. This period is used as all imagery from PlanetScope was captured within these times.

Synchronous satellite imagery over these sites was then downloaded from PlanetScope using a custom area of interest of the site and date range. The four band PlanetScope satellite imagery was then selected, subject to an initial visual inspection checking for cloud cover or other visual errors over the site. The imagery was then downloaded, and a metadata extraction script was used to extract the appropriate metadata (shown in Appendix A). The relevant metadata consists of the filename, reflectance coefficient, band harmonisation factor, offset factor, date, time, cloud cover (%), and unusable data (binary). The unusable data value is a binary value used to check for the presence of the unusable data mask automatically calculated by PlanetScope, present if large visual shifts or data corruption has occurred. The reflectance coefficient, band harmonisation factor, and offset factor are all used in the conversion from digital numbers of pixel reflectance, to top of atmosphere reflectances. Cloud cover is given as a percentage and is a measure of the total cloud cover of the scene. The date and time undergo further processing to convert from UTM to New Zealand's time zone, GMT+12/13, also accounting for daylight savings.

4.2 - Estimation of Turbidity

PlanetScope imagery is a ToA level product meaning it already has atmospheric corrections applied and a relative spectral response curve fitted. Thus, no further corrections must be made before the estimation of turbidity.

The turbidity equation used, equation 1, was also used by Vanhellemont (2019). It was developed by Nechad et al. (2010) as a generic multisensory algorithm for the mapping of total suspended solids in turbid waters. Thus, it is not specifically designed for estimating turbidity in specific environments such as estuarine or coastal waters but is more generic and should produce more accurate estimates in a wider range of applications. It is unique in that Nechad's equation is the only semi-empirical equation that doesn't require initial in-situ measurements to derive a turbidity relationship from readings (Dogliotti et al., 2015). All other equations are better described as indexes, requiring a relationship between factors such as suspended solids, chlorophyll-a concentrations, and reflectance, to estimate further turbidity readings for reflectance values.

$$T = \frac{A \cdot p_w}{1 - \frac{p_w}{C}} + B \quad (FNU) \qquad (1)$$

From equation 1, T is turbidity in FNU and p_w is the top of atmosphere water reflectance corrected for atmospheric interference. A, B and C are coefficients derived from the closest wavelength to the central wavelength of the band. Using band-weighted wavelengths is an alternative method and could produce more accurate results, but during testing by Nechad et al. (2010) little difference was noted. Figure 2 describes the appropriate coefficients for the central wavelength of any given measured band, while Table 2 describes the appropriate coefficients for PlanetScope imagery.

Table 2 - *Appropriate coefficients for the analysis of PlanetScopes data different bands*

Band	Wavelength (nm)	A	B	C
Green (B2)	500-590	122.15	3.32	53.7
Red (B3)	590-670	229.45	2.32	74.9
NIR (B4)	780-860	1664.01	1.65	77.3

To extract p_w, the respective images must first be imported into ArcMap for processing. Five points at the location of the sensor were then created, from which the average pixel brightness values (digital numbers) for each band are extracted using the multi-values to points tool. The narrower the waterway the less 'bunched' these points are to ensure different pixels are sampled. These extracted digital numbers are then exported to Excel and the five results for each respective band are averaged. This digital number is then converted to p_w using equation 2.

$$p_w = (\mathrm{DN}_{avg} \times \text{reflectance coefficient} \times \text{band harmonisation factor}) + \text{offset} \qquad (2)$$

Where DN_{avg} is the average digital number for an image, and other factors (derived from metadata) are used to transform the digital numbers to make them comparable across different sensors or satellites (Planet, 2016). Equation 1 was then used to estimate turbidity. The estimated turbidity was then compared to the synchronous in-situ sensor turbidity readings. If multiple images are taken on a single day, the values are averaged across the image, while analysis of individual turbidity readings will also be completed.

λ (nm)	A^ρ	B^ρ	R_ρ^2 %	λ (nm)	A^ρ	B^ρ	R_ρ^2 %	λ (nm)	A^ρ	B^ρ	R_ρ^2 %	λ (nm)	A^ρ	B^ρ	R_ρ^2 %
				600.0	155.61	2.87	68.6	700.0	445.11	1.13	82.5	800.0	1596.41	1.58	77.5
				602.5	162.61	2.90	70.0	702.5	468.13	1.15	82.6	802.5	1573.61	1.61	77.7
				605.0	174.82	2.83	71.1	705.0	493.65	1.16	82.8	805.0	1562.74	1.63	77.8
				607.5	184.42	2.69	71.9	707.5	526.68	1.15	82.9	807.5	1552.21	1.64	77.7
				610.0	191.73	2.66	72.4	710.0	561.94	1.23	82.9	810.0	1548.63	1.65	77.7
				612.5	198.36	2.54	72.9	712.5	606.12	1.19	82.9	812.5	1552.99	1.65	77.8
				615.0	203.69	2.53	73.2	715.0	649.78	1.25	82.7	815.0	1570.74	1.64	77.6
				617.5	208.81	2.52	73.6	717.5	708.16	1.17	82.5	817.5	1613.05	1.59	77.7
520.0	167.69	2.83	53.8	620.0	213.55	2.42	73.9	720.0	774.27	1.17	82.2	820.0	1664.01	1.65	77.3
522.5	161.48	2.87	53.8	622.5	217.73	2.42	74.2	722.5	861.11	1.16	82.0	822.5	1763.64	1.58	76.6
525.0	162.17	2.72	53.8	625.0	221.78	2.42	74.4	725.0	966.39	1.12	81.7	825.0	1867.44	1.60	75.9
527.5	155.27	2.89	53.7	627.5	225.15	2.42	74.7	727.5	1086.85	1.07	81.2	827.5	1996.74	1.60	74.7
530.0	148.37	2.97	53.7	630.0	229.45	2.32	74.9	730.0	1229.15	1.02	80.4	830.0	2125.12	1.72	73.4
532.5	147.68	2.87	53.7	632.5	234.85	2.30	75.3	732.5	1374.86	0.98	79.5	832.5	2267.88	1.71	72.1
535.0	140.09	3.07	53.7	635.0	239.94	2.29	75.6	735.0	1491.46	1.06	78.5	835.0	2379.77	1.80	70.8
537.5	138.71	2.99	53.7	637.5	245.08	2.28	75.9	737.5	1592.19	1.09	77.6	837.5	2481.42	1.83	69.7
540.0	130.43	3.21	53.7	640.0	249.96	2.26	76.2	740.0	1664.72	1.14	76.7	840.0	2543.56	1.92	68.5
542.5	129.74	3.11	53.7	642.5	254.60	2.24	76.5	742.5	1725.83	1.12	76.1	842.5	2601.28	1.93	67.7
545.0	122.15	3.32	53.7	645.0	253.51	2.32	76.7	745.0	1754.77	1.22	75.6	845.0	2646.87	2.00	67.0
547.5	121.46	3.23	53.9	647.5	260.09	2.20	77.0	747.5	1781.18	1.24	75.3	847.5	2697.96	2.00	66.4
550.0	120.77	3.14	53.9	650.0	268.95	2.17	77.2	750.0	1804.05	1.27	75.0	850.0	2719.82	2.08	65.8
552.5	113.17	3.44	54.0	652.5	280.36	2.14	77.6	752.5	1815.54	1.27	74.5	852.5	2780.02	2.03	65.4
555.0	111.79	3.35	53.9	655.0	289.29	2.10	77.9	755.0	1822.38	1.28	74.3	855.0	2814.06	2.12	64.8
557.5	104.89	3.60	53.8	657.5	307.78	1.96	78.2	757.5	1789.22	1.30	74.6	857.5	2870.40	2.11	64.2
560.0	104.20	3.47	53.7	660.0	327.84	1.91	78.5	760.0	1750.72	1.34	74.7	860.0	2905.11	2.21	63.8
562.5	97.30	3.74	53.5	662.5	342.56	1.84	78.7	762.5	1736.96	1.39	74.9	862.5	2924.54	2.28	63.1
565.0	97.99	3.62	53.4	665.0	355.85	1.74	78.9	765.0	1795.66	1.38	75.5	865.0	2971.93	2.30	62.7
567.5	91.78	3.92	53.3	667.5	374.11	1.61	79.1	767.5	1851.11	1.41	75.3	867.5	3016.31	2.32	61.9
570.0	93.16	3.74	53.3	670.0	384.11	1.44	79.4	770.0	1894.33	1.37	75.3	870.0	3050.06	2.40	61.2
572.5	89.02	3.97	53.5	672.5	391.38	1.26	79.7	772.5	1889.64	1.43	75.3	872.5	3104.12	2.45	60.7
575.0	93.16	3.72	54.1	675.0	401.61	1.09	80.0	775.0	1866.93	1.47	75.1	875.0	3161.90	2.46	60.0
577.5	93.16	3.78	55.2	677.5	403.49	1.04	80.4	777.5	1834.05	1.53	75.2	877.5	3199.96	2.58	59.1
580.0	95.92	3.74	56.7	680.0	408.84	0.82	80.7	780.0	1802.62	1.57	75.3	880.0	3251.89	2.65	58.4
582.5	98.68	3.73	57.8	682.5	400.68	0.87	81.0	782.5	1787.56	1.50	75.5	882.5	3318.38	2.65	57.6
585.0	80.74	4.34	54.3	685.0	396.87	0.84	81.3	785.0	1760.19	1.54	75.7	885.0	3388.53	2.68	56.6
587.5	84.19	4.37	56.6	687.5	394.57	0.85	81.5	787.5	1724.54	1.59	76.0				
590.0	93.85	4.08	59.1	690.0	394.20	0.90	81.7	790.0	1701.46	1.54	76.3				
592.5	109.72	3.58	61.9	692.5	402.74	0.96	81.9	792.5	1667.30	1.58	76.6				
595.0	124.91	3.26	64.5	695.0	414.72	1.02	82.1	795.0	1646.43	1.53	76.9				
597.5	138.02	3.14	66.8	697.5	430.21	1.08	82.3	797.5	1619.05	1.56	77.3				

Figure 2 - *Coefficients for determination of turbidity relative to central wave length (Nechad et al., 2010).*

5. Results

5.1 - Overview

The turbidity of the four data collection sites was estimated using satellite imagery from the PlanetScope Array. The time periods over which turbidity was estimated for each site were selected based on the in-situ data. Comments on the data (based on comparison to laboratory water sample testing) were used to determine a two- to four-month period in which the in-situ data was most likely to be accurate. Common errors that could occur with in-situ data collection include smearing of the sensor lens, battery power running out or the water level decreasing below the sensor level. For each data collection site and respective time period, satellite imagery was downloaded from PlanetScope. The number of images and data collection period for each site are shown in Table 3.

Table 3 – *Waterway, data collection period and the number of images turbidity estimated from by site.*

Site	Waterway	Data Collection Period	No. of Images
Site A	Waikato River	15/12/2020 - 14/02/2021	47
Site B	Waikato River	5/2/2020 - 25/5/2020	60
Site C	Heathcote Stream	N/A	N/A
Site D	Heathcote Stream	15/12/2020 - 8/2/2021	34

Within these results the most appropriate band for estimating turbidity was first determined, then the results of estimating turbidity at each site are reported on a site-by-site basis. Initially, an overview of the data and characteristics of each site are shown, followed by a more in-depth analysis of interesting points for the site. Points of interest include events such as large peaks of in-situ turbidity, or where there are large discrepancies between estimated and in-situ turbidity. Finally, a linear regression analysis of each site is discussed.

There was significance variance of in-situ readings over the period of 25 days, 14/12/2020 to 7/1/2021 at site A. The average standard deviation of readings was 0.91 with a mean of 5.71FNU. The satellite imagery used is only captured between the periods of 9am and 1pm, thus, the in-situ reading for a day will be taken as the average of this period. In the same period this reduced the standard deviation to 0.56, with a mean of 5.22FNU. This level of accuracy is sufficient for this project, but future research could consider taking the nearest in-situ reading if more precise readings were required.

5.2 - Band Comparison

Before turbidity was estimated for all the sites, the most appropriate (accurate) band was determined. This was completed by comparing the estimated turbidity of each band to the in-situ turbidity for the Site A dataset. Note that of the four bands of PlanetScope's imagery, the blue band (455-515 nm) is not used as its central wavelength is below the range acceptable for use in Nechad's equation (Equation 1). The comparison used an average of five sampling points at the location of the in-situ sensor at Site A, as shown below in Figure 3. Table 4 shows the average estimated turbidity values for the green, red and NIR bands of the PlanetScope imagery and the average in-situ value from 15/12/2020 to 14/02/2021.

Figure 3 - *Site A sampling points and location.*

Table 4 - *Average estimated and in-situ turbidity values for site A from 15/12/2020 to 14/02/2021.*

	Average Turbidity (FNU)
Green Band	4.96
Red Band	5.44
NIR Band	63.19
In-situ average	4.48

From Table 4 it is shown that the NIR band consistently estimated values that were an order of magnitude higher than both the other bands and the in-situ turbidity averages. Thus, the other bands produce more accurate estimates of turbidity and the NIR band will not be used. This was expected, as the NIR band is not often used for remote water sensing applications, and Vanhellemont (2019) noted radiometric inconsistencies of 40% in the NIR for near-simultaneous images of the PlanetScope array.

To compare the appropriateness of the green and red bands, the estimated turbidity of each band for each image has been compared to the respective in-situ turbidity. This is shown in Figure 4, which additionally plots the average of the red and green estimated turbidities for comparison. It shows that each band follows the same trend, this is to be expected as the bands simply change the coefficients used in Nechad's equation (Section 4.2). Thus, the red band is more sensitive to changes in turbidity, with peaks being higher and troughs lower. The green band is typically less sensitive to the changes in turbidity, with less variation. Finally, when the estimated turbidity for each day was compared to the closest in-situ measurement (15-minute intervals), the green band was more accurate in 25 out 38 occasions, or 66% of the instances. Therefore, the green band was used preferentially throughout the remainder of the analysis.

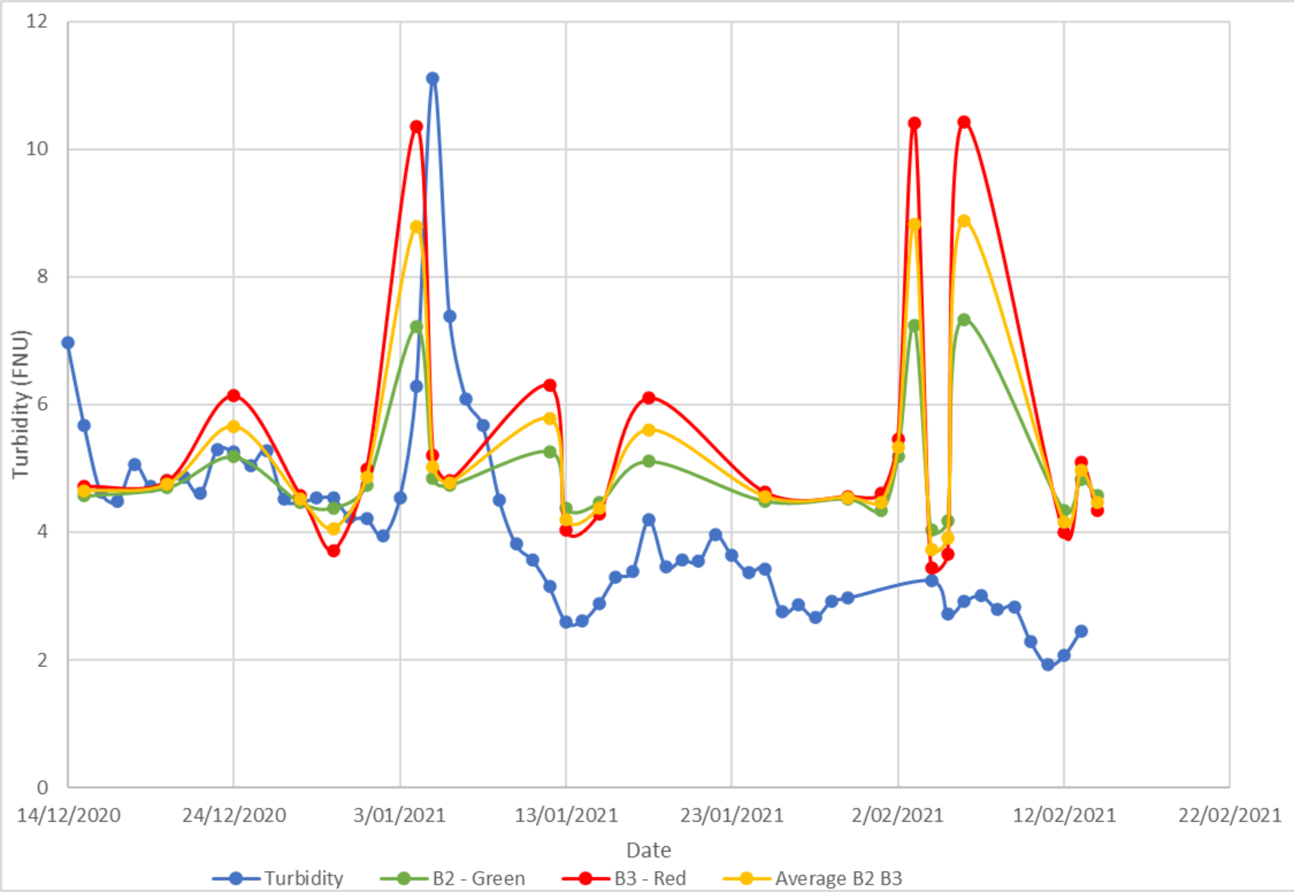

Figure 4 – *Comparison of different bands estimation of turbidity for site A from 15/12/2020 to 14/02/2021.*

5.3 - Site A

Site A is in the Waikato River near the outlet at Port Waikato, at a point where the waterway is both deep and wide. The sampling points for this are shown in Figure 4. The in-situ measurements and estimated turbidity from 15/12/2020 to 14/02/2021 are shown in Figure 5. Firstly, note that the turbidity of the river was typically quite low with the maximum difference in in-situ turbidity of 7.0FNU. Small changes in turbidity are both harder to detect and less likely to have negative environmental effects (this characteristic applies to all sites). Overall, the satellite estimation of turbidity follows the same trend as the in-situ data, although it does differ at several key points.

The satellite data has successfully identified the initial increase in turbidity at point A but underestimated it the following two days. From the 4/1/2021 to 6/1/2021, imagery was available every day to estimate turbidity. On each of these days, there were three separate images analysed; these results are shown in Table 5. Firstly, note that the near synchronous images from different satellites are achieving very similar estimates for turbidity, well within the expected margin of error. However, although consecutive images are estimating turbidity consistently, it consistently underestimates the magnitude of the increase. Figure 4 shows this occurred across all bands and is not confined to the green band.

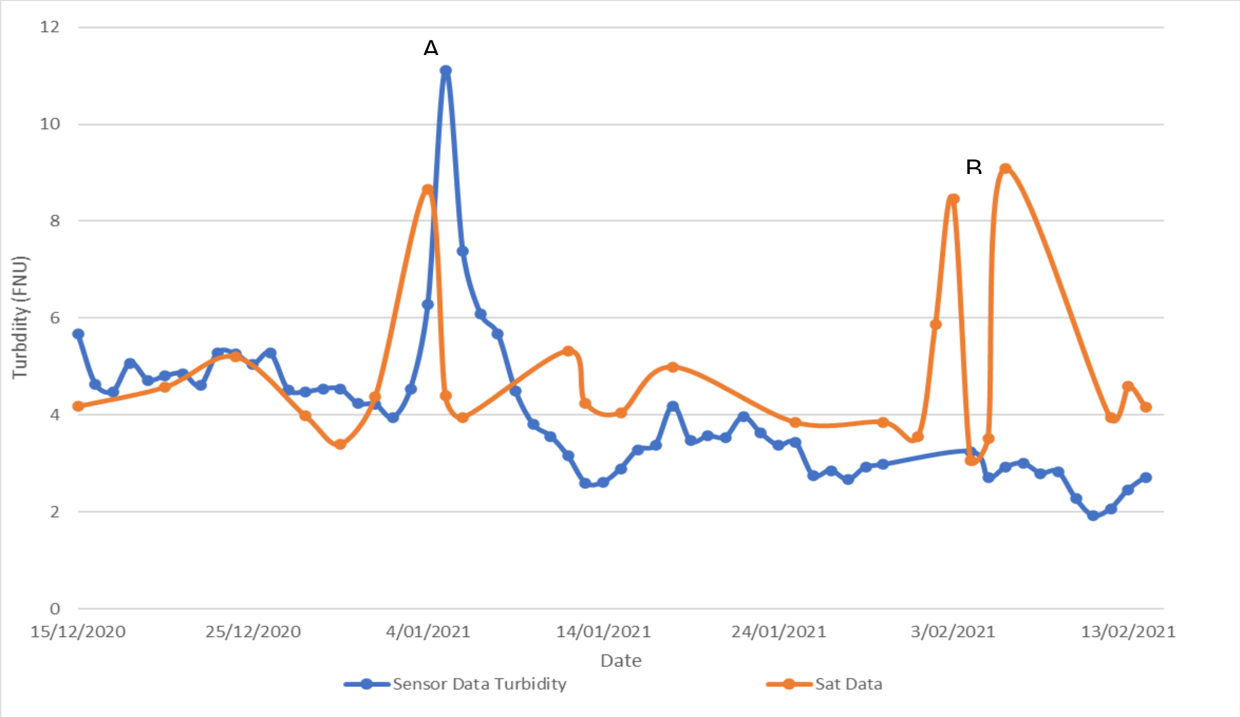

Figure 5 - *Site A in-situ turbidities compared to estimated turbidities from 15/12/2020 to 14/2/2021.*

The satellite data also identified two further peaks (point B) on the 3/2/2021 and 5/2/2021. On the 3/2/2021 there was no in-situ sensor data available, thus, this peak is not able to be verified. However, there is a large difference between the two estimations of turbidity made on the 3/2/2021, with measurements of 4.32 FNU and 10.14 FNU. Thus, it is likely that the second estimation is incorrect and skewing the average for the day. The estimation on the 6/2/2021 is also likely incorrect, but due to it being the only imagery available on the day it is not able to be compared to other estimations. Note that both these estimations differ considerably from the average estimated turbidites on the 4/2/2021 and the 5/2/2021. It is not apparent why these overestimations occurred, with minimal cloud cover in the images and no visual shifts in colour.

Table 5 – *Estimated and in-situ turbidity readings for Site A from the 4/1/2021 to 6/1/2021.*

		Turbidity	
Date	**Time**	**Estimated (FNU)**	**In-situ (NTU)**
4/01/2021	11:40:36 AM	8.6	6.3
4/01/2021	11:40:38 AM	8.5	6.3
4/01/2021	12:23:25 PM	4.5	5.6
5/01/2021	9:54:01 AM	5.0	9.9
5/01/2021	9:54:02 AM	5.0	9.9
5/01/2021	11:26:10 AM	4.5	12.8
6/01/2021	11:28:11 AM	4.7	7.1
6/01/2021	11:28:14 AM	4.7	7.1
6/01/2021	12:23:19 PM	4.8	7.1

The linear regression analysis of the results of site A is shown by Figure 6, which has two series, a first with all data points, and a second series with the two obvious outliers removed. This shows quite a weak relationship between the measured and in-situ turbidity for both data sets, although removing outliers increased the goodness of fit. Note that a stronger relationship between the trends would have a 1:1 trend of data points, where the estimated turbidity is the same as the in-situ turbidity. The intercept of these trend lines for all data points was 4.36FNU, which shows the bias of Nechad's equation to overestimate turbidity in this application.

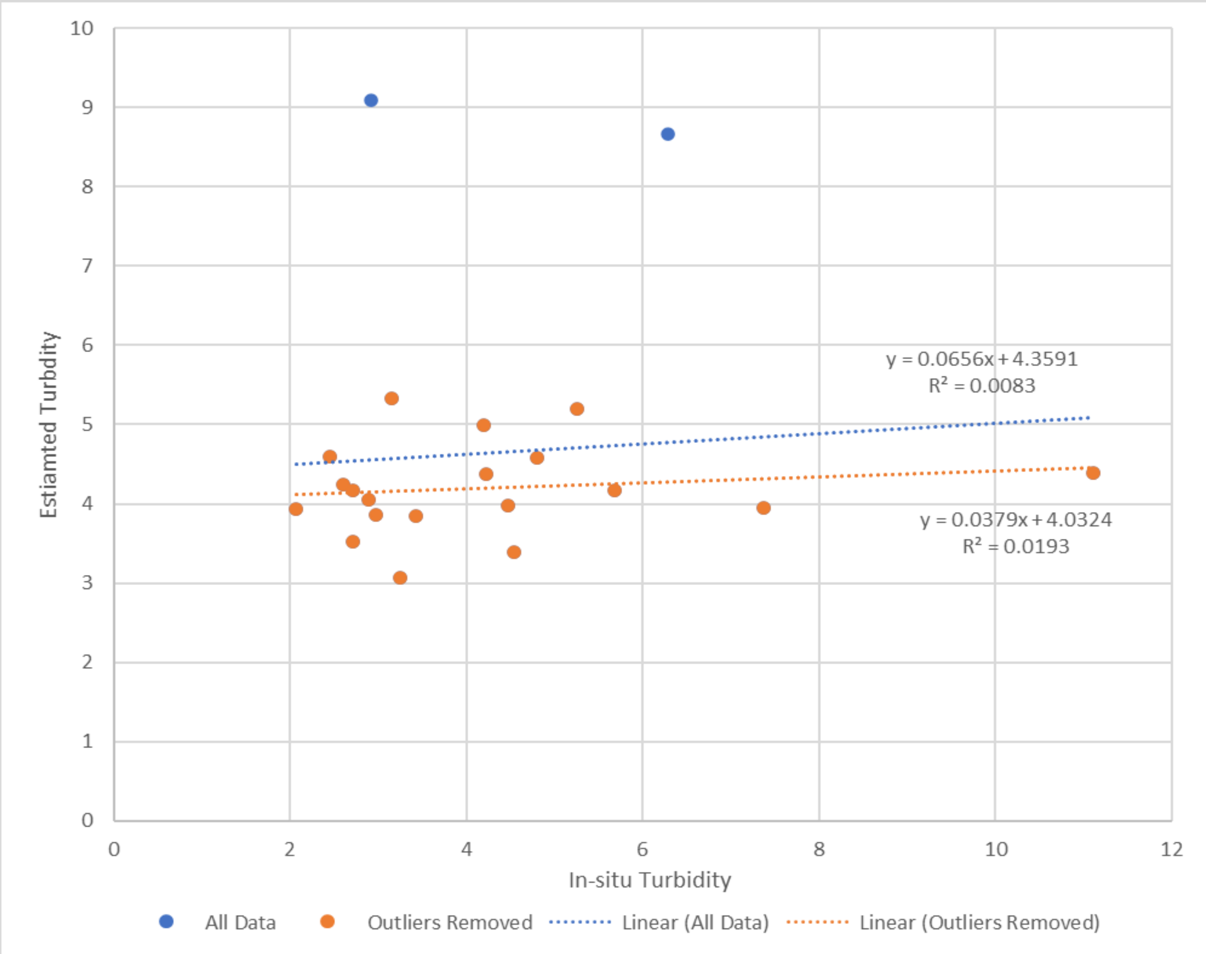

Figure 6 - *Linear regression analysis of Site A.*

5.4 - Site B

Site B is in the Waikato River near Hamilton City centre, again at a relatively wide and deep point of the river. The sampling points and location are shown in Figure 7. Turbidity was estimated for imagery from the 5/2/2020 to 25/5/2020, with the results of this shown in Figure 8. Overall the satellite consistently overestimated turbidity, especially at the lower turbidity levels, but the general trend of the in-situ readings is reflected by the estimated turbidities. This is most apparent at the increase of turbidity levels at points B, C, and D. At these points, the in-situ readings increased, and an increase of relatively the same magnitude was observed in the estimated turbidities

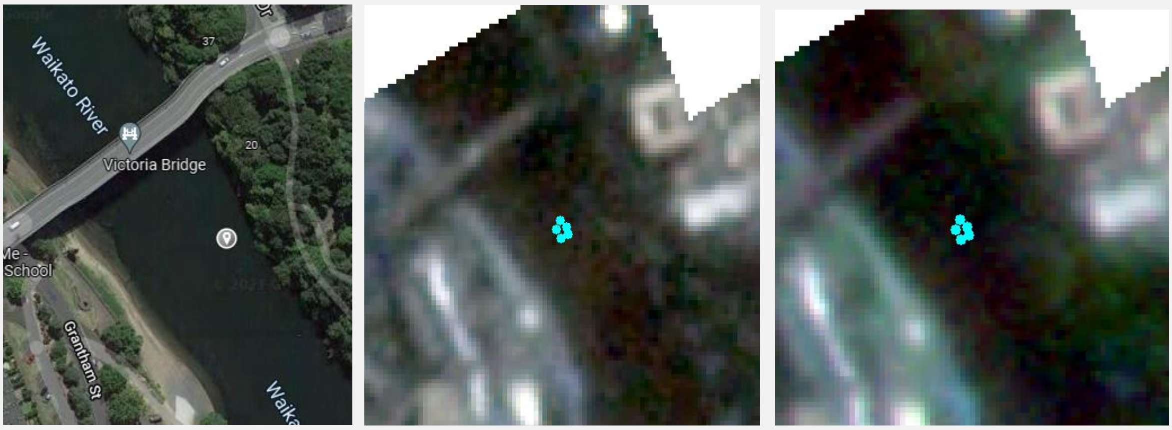

Figure 7 - *Site B sampling points, location and images of peak at point E.*

At point A there are two large peaks in estimated turbidity of 5.99 and 6.08 FNU; both were derived from single images with no obvious visual shifts in colour and cloud cover percentages of 12.8% and 50.6% respectively. The in-situ data readings were consistent with the average readings at the times these images were taken. At point B there is another peak in turbidity on the 30/3/2020, once again there is no obvious visual shift in colour, however, cloud cover was significant at 79.4%. Cloud cover is likely affecting the estimation of turbidity in these images.

Point E is taken as the average of two turbidity estimations of 7.88 and 7.71 FNU which is significantly higher than the in-situ readings. However, once again there are no obvious visual shifts in colour and cloud cover of 3% and 0% respectively. These images were taken 30 minutes apart and are shown in Figure 7. It is unknown why both images are overestimating turbidity.

The linear regression analysis of site B is shown by Figure 9. The relationship between the estimated and in-situ turbidity is better than Site A, trending closer to a 1:1 relationship. The goodness of fit is also much better, with a R^2 value of 0.254. The intercept of trend is 3.33 FNU, showing the bias of the estimation method to overestimate. A two-sample t-test with equal variance was also completed, resulting in a two-tail P-value of $2.5e^{-18}$, or very significant (<0.05). This means that it is very unlikely that the observed correlation between the estimated and in-situ turbidities was simply a function of chance.

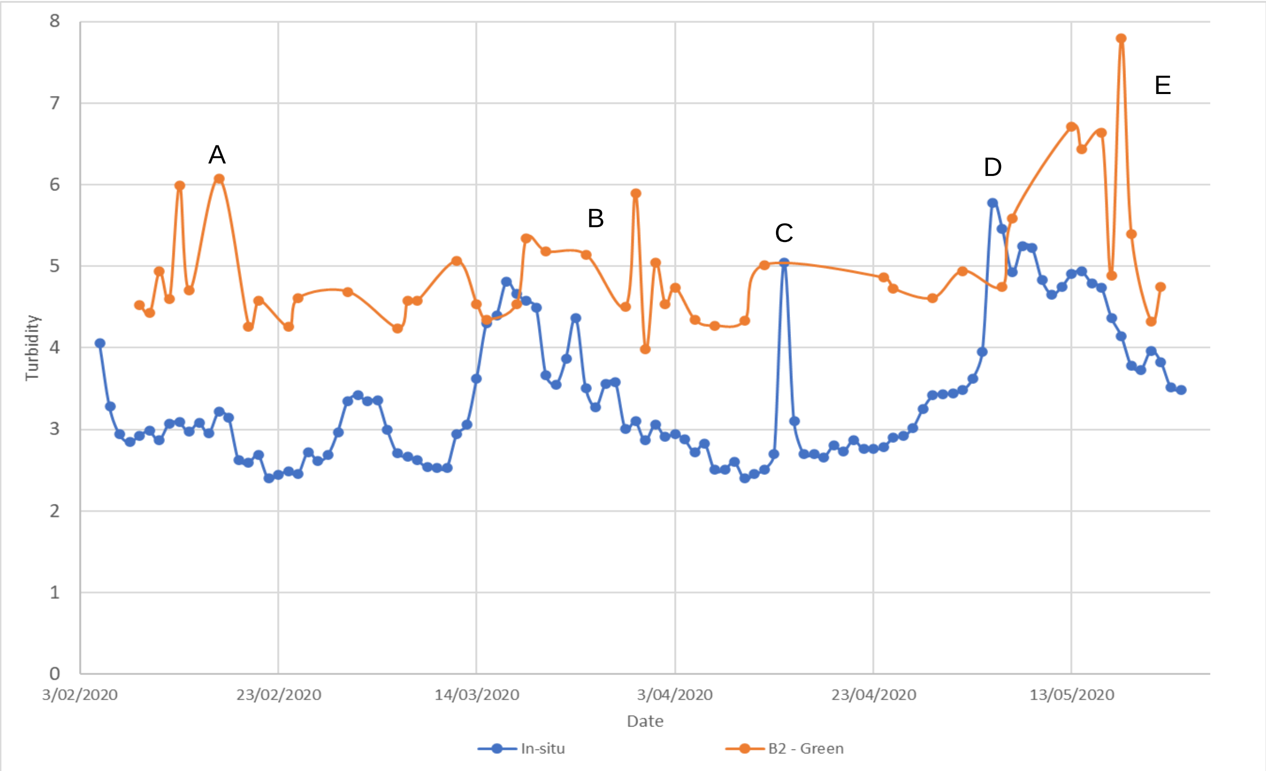

Figure 8 - *Site B in-situ turbidities compared to estimated turbidities from 5/2/2020 to 25/5/2020.*

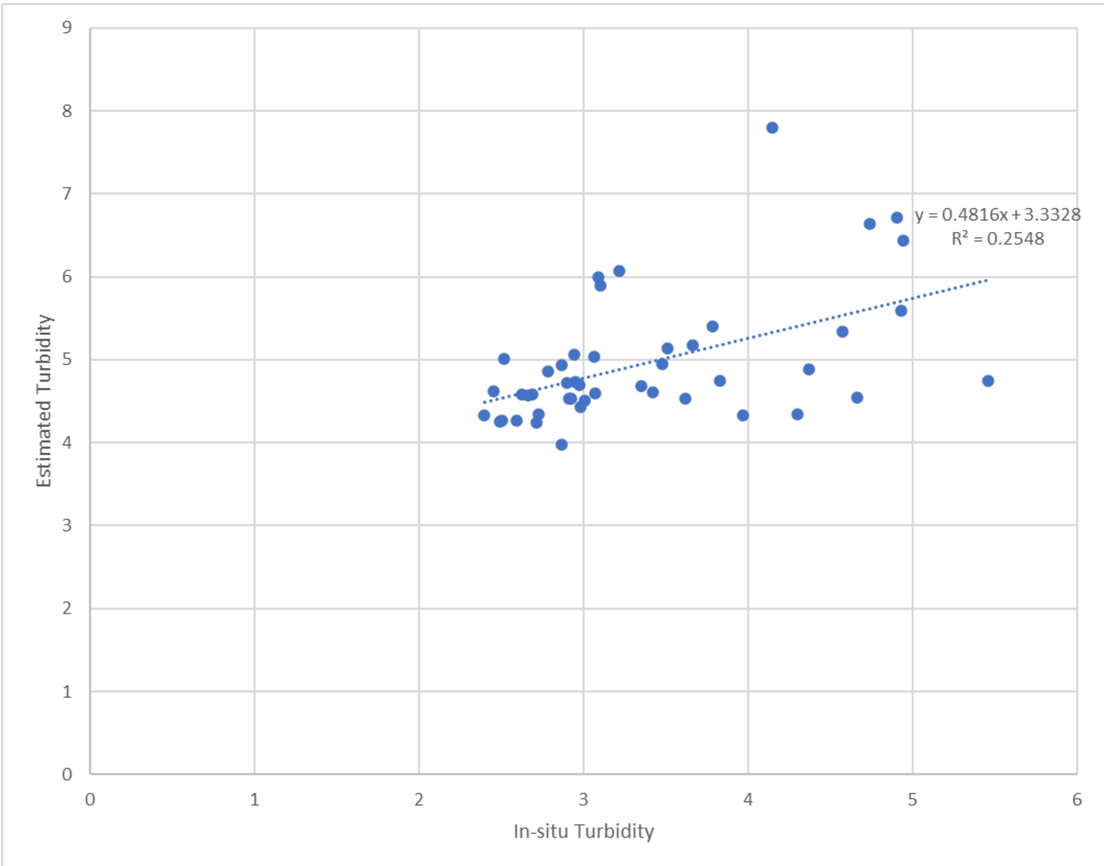

Figure 9 - *Linear regression analysis of site B.*

5.5 - Site C

Site C is in the Heathcote Stream near Cashmere and has a width of 8m at the in-situ sampling point. However, the overhanging trees mean that the effective width of the waterway, when viewed on satellite imagery, is less than three metres. Thus, Site C showcases the limitations of remote turbidity sensing in that the portion of the waterway visible from the sky must be large enough to enclose a single pixel (3x3 m for PlanetScope imagery). Thus, it is not possible to estimate turbidity at Site C as the waterway cannot be discerned from the imagery. This is shown in Figure 10, with the google maps imagery, which is artificially enhanced for reference, and two different PlanetScope images by comparison. A waterway that was more suited to this method of turbidity estimation would ideally be wider and with less cover from the surrounding environment. However, if there was a pool or wide bend of a waterway that met the above conditions, this could also be used. Alternatively, higher resolution imagery could be considered.

Figure 10 - *Site C imagery comparison between Google (left) and Planet Scope (center and right).*

5.6 - Site D

Site D is the Heathcote Stream near St Martins, downstream of Site C. This site is narrower in width than Site C at 6m, but it has significantly less tree cover allowing for turbidity estimation from PlanetScope imagery. The site and sampling points are shown in Figure 11. Images were analysed from 15/12/2020 to 8/2/2021 with the results shown against in-situ turbidity in Figure 12.

Figure 11 – *Site D sampling points and location (6.81 FNU pictured).*

Overall, the readings from site D are very consistent but fail to identify any peaks in the data. This however cannot be attributed solely to Nechad's equation, but rather the lack of imagery available for analysis during these periods of increased turbidity. The most significant outlying estimation was on the 24/01/2021 with a value of 6.81 FNU. The image for this estimation is shown in Figure 10 and is without any visually apparent issues with geolocation or colour shift. However, metadata shows the overall scene to have a cloud cover of 16%. This is not significantly greater than other imagery but illustrates the possibility that cloud cover has affected the turbidity estimation.

Figure 13 shows the linear regression analysis of Site D, which has a relatively weak relation between estimated and in-situ turbidity. However, the interception of the trend line is consistent

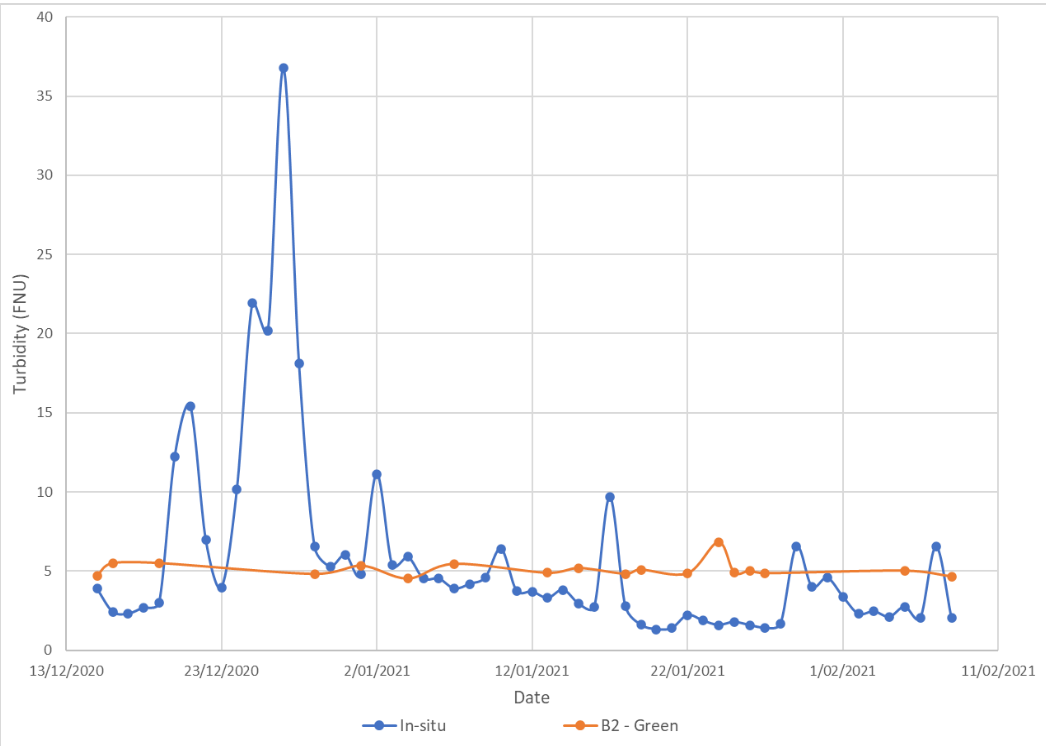

Figure 12 - *Site D in-situ turbidities compared to estimated turbidities from 15/12/2020 to 8/2/2021.*

with the other sites at 5.27 FNU, again showing the bias to overestimate. The R^2 value is also relatively high at 0.191, with better goodness of fit than Site A.

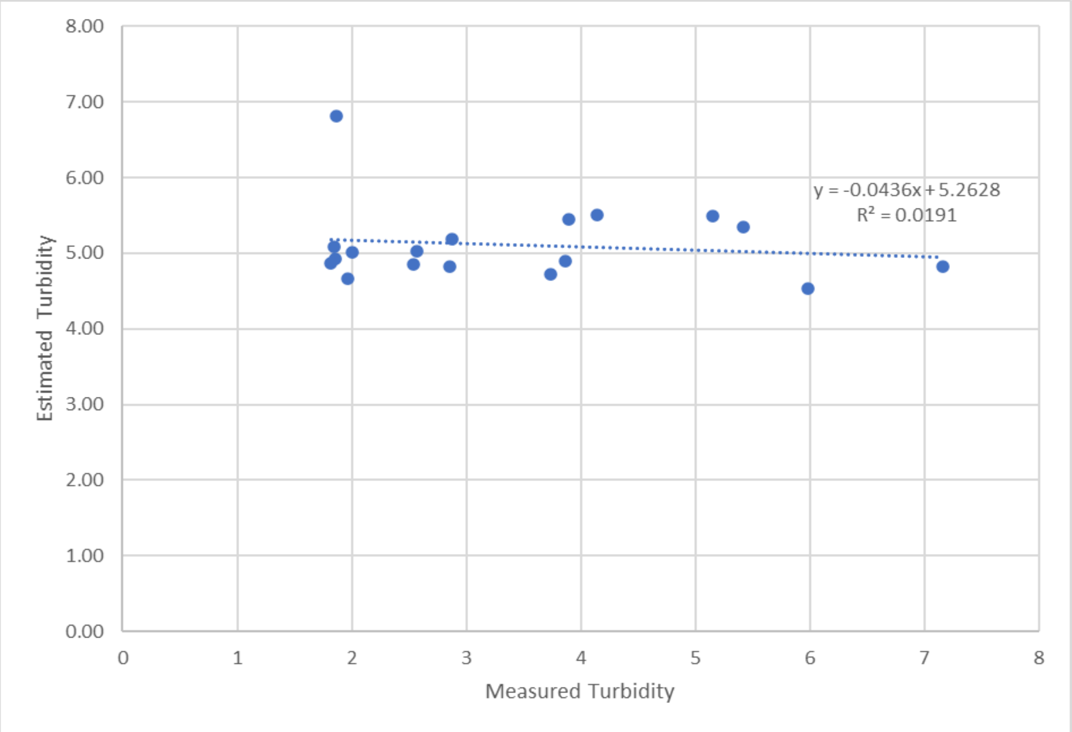

Figure 13 – *Linear regression analysis for Site D.*

6. Discussion

6.1 – Potential of Remote Turbidity Estimation Applications

The objective of this report is to assess the potential of using remote sensing to determine the turbidity of waterways within New Zealand. The equation used for this, Nechad's equation, was originally designed for use in coastal waters of low to moderate turbidity. Thus, this study represents a non-intended use case of the equation. However, it is still a valid choice in that it is the only equation that does not require initial in-situ testing to estimate turbidity. Coastal waters differ from inland waters in their salinity, algae concentrations, sediment type and the absorption of light by phytoplankton. These factors affect the backscattering and reflectance of light, thus changing the estimated turbidity. Therefore the implementation of this method is not as accurate as other studies such as Dogliotti et al. (2015), who achieved a mean relative error of 13.7% across their dataset of 106 locations. This level of accuracy achieved within this study was much less than this.

However, the absolute value of the turbidity measurement may be viewed as inherently less important than the relative change of it. That is, increases in turbidity above 30% influence the aesthetic and safety aspects of contact recreation (Ministry for the Environment, 2002), as well the environmental effects discussed in the introduction. The results show that changes in turbidity can be detected if appropriate imagery and sampling locations are available, with the identification of peaks in turbidity on sites A and B being good examples of this. Thus, I propose that the ideal use of this technology is as a precursor to the use of more expensive, in-situ sampling methods, in identifying the locations that may require attention. It allows for the development of a dataset with very fine spatial extent, but coarse temporal extent at a relatively low cost. The accuracy of measurements will not be as good as in-situ measurements, but the spatial extent of the dataset is unparalleled when compared on a cost basis to other sampling methods.

A possible implementation includes the monitoring of an entire length of a waterway. For example, sampling points could be placed in intervals along the length of a waterway, and changes in turbidity along the length could be observed. This could allow for the determination of point sources of pollution at scales unreasonable with in-situ testing. The technology could also be implemented for the wide-scale monitoring of lakes, regardless of the ease of access. Note that a similar tool is being developed by Seequent currently. Both these implementations of the technology could allow for 'problem' areas with unreasonably high turbidities or large changes occurring to be identified. This would allow the problem areas to be investigated further and the implementation of measures to protect and retain water quality.

6.2 – Factors Influencing Estimation of Turbidity

The most significant factor in determining turbidity is the requirement of having a single, unobstructed water pixel visible within the imagery. This is shown by Site C, where the overhanging vegetation and narrowness of the river prevented this. The required size of this pixel is determined by the spatial resolution of the imagery, where PlanetScope imagery is 3x3m. From comparison of the sites, the greater the width of the waterway, the easier it is to estimate turbidity; both Waikato River sites were much easier to locate the sampling points within compared to the Heathcote Stream. Furthermore, if the imagery has issues with geolocation and inconsistent ground control points (which can be common) the wider the waterway, the more allowance for error before the sampled pixels are not entirely water. Thus, sites A and B are examples of ideal applications for the technology, Site D was marginal and Site C was simply not achievable. Note that finer resolution imagery would allow for narrower waterways to be sampled.

The second most significant factor is the availability of imagery. This is affected by weather, site location and required spatial resolution of the imagery for the site. Imagery is only suitable for estimating turbidity from if the sampled pixels are fully visible and uninterrupted by clouds or vegetation. Site location will often affect the temporal resolution of imagery available, for example, sites near major cities or with higher population densities are more likely to have imagery available as there is a higher demand for imagery of the location. For the spatial resolution of the imagery, as the requirements increase, the availability of imagery at desired resolution decreases, and the cost often increases significantly. These factors mean that New Zealand is not ideal for remote image acquisition compared to other countries. The low population results in lower demand for imagery and it's Māori name, Aotearoa, or the 'land of the long white cloud' holds true in image acquisition opportunities. Therefore, the temporal resolution of data sets is location dependant, but New Zealand faces relatively difficult conditions compared to other countries. A further result of this is the difficulty in identifying peaks in turbidity. These peaks are often associated with adverse weather events such as rain or storms, both of which are accompanied by cloud cover, making turbidity estimation impossible. This is an inherent weakness of the technology/method and cannot be overcome.

Several environmental factors can also affect the estimation of turbidity such as cloud cover, the sun zenith angle, and the viewing angle of the satellite. The sun zenith angle and viewing angle were not analysed as other factors were determined to have a much large effect on accuracy. However, Dogliotti et al. (2015) noted their mean relative error within their estimations increased by up to 7% as the viewing and zenith angles increased. Within the results, many of the outlying results were estimated using imagery with high cloud cover percentages. This occurs because the cloud intercepts the part of the light, scattering the rays resulting in less light reaching the sensor. Thus, it mimics the effects of sedimentary particles in water, meaning turbidity estimations are overestimated. This is most aptly shown by Site B, at points A and B.

6.3 – Overestimation of Turbidity

The base flow turbidity levels are consistently overestimated at all sites. This was demonstrated with a positive bias in estimations across all linear regressions, with an average bias across all sites of 4.32 FNU. This is most likely due to the calibration of Nechad's equation for moderately turbid coastal waters. As the in-situ turbidites are much lower than the waters it was calibrated for, it tends to overestimate. For Nechad's equation (section 4.2) a constant is added to a function, where the function is always positive. This means that no matter what reading, the minimum turbidity level will be equal to the constant, or 3.32 FNU for the green band. The effect of this is especially apparent in sites B and D, where the baseflow turbidities are often below 3.32 FNU.

It is possible that the reduction of this constant would allow for turbidity to be estimated more accurately. However, this reduction would be site-specific and estimated turbidity must be correlated against in-situ measurements. This site-specific approach would defeat the purpose of a semi-empirical, generic approach. Thus, a better approach would be to recalibrate the equation for freshwater waterways as discussed in Section 6.4.

6.4 – Future Research Opportunities

Perhaps the most significant research opportunity is the recalibration of Nechad's equation for freshwater, or New Zealand waterways. The results above have shown that changes in turbidity can be detected, although the accuracy of turbidity measurements could be improved. This would involve non—linear regression analysis of in-situ water reflectances and appropriate, simultaneous satellite imagery (Nechad et al., 2010). Nechad et al. (2010) further noted that the variability between different geographic regions is significant, although the studied area (Southern North Sea) was a widely variable region that is representative of many other regions. By creating a model that is calibrated for freshwater waterways it allows for much more representative estimations of turbidity.

Other possible research future research opportunities lie in the application of this method to a much larger range of waterways and lakes, or implementation along the length of a waterway. The determining factor in the ability to do this would be the availability of in-situ data to check the validity of the estimations. However, if it was shown that changes in turbidity could be reliably identified and long-term trends can be observed, it could allow for the better management of our water resources and increased efficiency when allocating resources to ensure they are used where they are needed most.

6. Conclusion

Through the comparison of in-situ turbidity measurements to estimated turbidites from satellite imagery in New Zealand waterways, this dissertation has shown that there exists a large potential for remote sensing applications in turbidity sensing. Key findings show that the method can identify changes in turbidity providing that appropriate imagery is available, although the accuracy of individual estimations could be improved. The wider the waterway, the easier it is to estimate turbidity from, with the spatial resolution of satellite imagery acting as the defining constraint.

The areas of application for this technology are likely in the assisting of in-situ testing, identifying areas of high turbidity or abrupt changes. It is possible that the recalibration of Nechad's equation for inland, freshwater waterways and lakes could result in more accurate estimations of turbidity. Other possible areas for future research include the application of the existing method to a wider range of areas and water bodies such as lakes, subject to the availability of in-situ measurement by which to correlate estimated results.

Key limitations of this method exist in the availability of imagery, spatial resolution, and calibration of Nechad's equation. An inherent limitation is the tendency of increased turbidity to occur during storm or rainfall events, or at the same time when cloud cover means imagery is not obtainable. Thus, the method is likely best used in conjunction with in-situ measurements.

Overall, this dissertation has that there is much potential in the application of remote sensing technologies in the turbidity monitoring of waterways. Further research is required for meaningful and consistent application of the technology, but the possibility of application has been shown.

7. References

Binding, C., Bowers, D., & Mitchelson-Jacob, E. (2005). Estimating suspended sediment concentrations from ocean colour measurements in moderately turbid waters; the impact of variable particle scattering properties. *Remote Sensing of Environment*, *94*(3), 373-383.

Campbell Scientific, I. (2014). *OBS-3+ and OBS300 Suspended Solids and Turbidity Monitors. In Instruction Manual.* http://s.campbellsci.com/documents/us/manuals/obs-3+.pdf

Chen, Z., Hu, C., & Muller-Karger, F. (2007). Monitoring turbidity in Tampa Bay using MODIS/Aqua 250-m imagery. *Remote Sensing of Environment*, *109*(2), 207-220.

Curran, P., & Novo, E. (1988). The relationship between suspended sediment concentration and remotely sensed spectral radiance: a review. *Journal of Coastal Research*, 351-368.

Davies-Colley, R., & Smith, D. (2001). Turbidity Suspended Sediment, and Water Clarity: A Review *JAWRA Journal of the American Water Resources Association*, *37*(5), 1085-1101.

Dogliotti, A. I., Ruddick, K., Nechad, B., Doxaran, D., & Knaeps, E. (2015). A single algorithm to retrieve turbidity from remotely-sensed data in all coastal and estuarine waters. *Remote Sensing of Environment*, *156*, 157-168.

Fondriest, E. (2014). Measuring Turbidity, TSS, and Water Clarity. Fundamentals of Environmental Measurements. In.

Gallegos, C. L., Correll, D. L., & Pierce, J. W. (1990). Modeling spectral diffuse attenuation, absorption, and scattering coefficients in a turbid estuary. *Limnology and Oceanography*, *35*(7), 1486-1502.

Groom, S., Sathyendranath, S., Ban, Y., Bernard, S., Brewin, R., Brotas, V., Brockmann, C., Chauhan, P., Choi, J.-k., & Chuprin, A. (2019). Satellite ocean colour: current status and future perspective. *Frontiers in Marine Science*, *6*, 485.

Hamill, K., & Lew, D. (2006). *Snapshot of lake water quality in New Zealand*. (0478301073). Ministry for the Environment

Isidro, C. M., McIntyre, N., Lechner, A. M., & Callow, I. (2018). Quantifying suspended solids in small rivers using satellite data. *Science of the Total Environment*, *634*, 1554-1562.

Kuhn, C., de Matos Valerio, A., Ward, N., Loken, L., Sawakuchi, H. O., Kampel, M., Richey, J., Stadler, P., Crawford, J., & Striegl, R. (2019). Performance of Landsat-8 and Sentinel-2 surface reflectance products for river remote sensing retrievals of chlorophyll-a and turbidity. *Remote Sensing of Environment*, *224*, 104-118.

McCabe, M. F., Aragon, B., Houborg, R., & Mascaro, J. (2017). CubeSats in hydrology: Ultrahigh-resolution insights into vegetation dynamics and terrestrial evaporation. *Water Resources Research*, *53*(12), 10017-10024.

Ministry for the Environment, M. (2002). *Microbiological Water Quality Guidelines for Marine and Freshwater Recreational Areas*

Nechad, B., Ruddick, K. G., & Park, Y. (2010). Calibration and validation of a generic multisensor algorithm for mapping of total suspended matter in turbid waters. *Remote Sensing of Environment*, *114*(4), 854-866.

Nisbet, T. (2001). The role of forest management in controlling diffuse pollution in UK forestry. *Forest Ecology and Management*, *143*(1-3), 215-226.

NZFOA, N. Z. F. O. A. (2015). New Zealand Environmental Code of Practice for Plantation Forestry. *New Zealand Forest Owners Association, Wellington, New Zealand*.

Pereira, L. S., Andes, L. C., Cox, A. L., & Ghulam, A. (2018). Measuring Suspended-Sediment Concentration and Turbidity in the Middle Mississippi and Lower Missouri Rivers Using Landsat Data. *JAWRA Journal of the American Water Resources Association*, *54*(2), 440-450.

Planet. (2016). *RapidEye Imagery Product Specifications*. https://www.planet.com/products/satellite-imagery/files/160625-RapidEye%20Image-Product-Specifications.pdf

RapidEye. (2012). *The RapidEye Red Edge Band*. https://apollomapping.com/wp-content/user_uploads/2012/07/RapidEye-Red-Edge-White-Paper.pdf

Reddy, P. (2017). *Resource management national environmental standards for plantation forestry regulations 2017*.

Research, N. I. o. W. A. (2020). *National River Water Quality Network*. https://niwa.co.nz/freshwater/water-quality-monitoring-and-advice/national-river-water-quality-network-nrwqn

SABD, S. A. s.-B. S. (2018). *Turbidity*. https://jackfife2000.wixsite.com/website-2/turbidity

Sadar, M. (2017). Turbidity measurement: A simple, effective indicator of water quality change. *OTT Hydromet. Retrieved from http://www. ott. com/en-us/products/download/turbidity-white-paper*.

Seequent. (2019). Seequent wins New Zealand aerospace innovation challenge; continues to expand its geoscience solutions to help solve earth, environment and energy challenges. https://www.seequent.com/satellite-based-lake-health-monitoring-system-an-aerospace-winner/

Seequent. (2020). *SLIMS Prototype* https://slimsprototype.web.app/#

Shen, F., Zhou, Y., Peng, X., & Chen, Y. (2014). Satellite multi-sensor mapping of suspended particulate matter in turbid estuarine and coastal ocean, China. *International Journal of Remote Sensing*, *35*(11-12), 4173-4192.

Tobin, A., Khan, A. A., Khan, H., Moores, L., & Taylor, J. (2007). Forestry Water Quality Index–A planning tool for the assessment and communication of the impacts of forestry activities on water quality. *The Forestry Chronicle*, *83*(2), 207-214.

Topp, S. N., Pavelsky, T. M., Jensen, D., Simard, M., & Ross, M. R. (2020). Research trends in the use of remote sensing for inland water quality science: Moving towards multidisciplinary applications. *Water*, *12*(1), 169.

Vanhellemont, Q. (2019). Daily metre-scale mapping of water turbidity using CubeSat imagery. *Optics express*, *27*(20), A1372-A1399.

Webb, A., & Haywood, A. (2005). Impact of Mitigated Forestry Activities on Turbidity.

Yigit Avdan, Z., Kaplan, G., Goncu, S., & Avdan, U. (2019). Monitoring the water quality of small water bodies using high-resolution remote sensing data. *ISPRS International Journal of Geo-Information*, *8*(12), 553.

8. Appendix A

```
"""
Report information:

The purpose of this is browse the file folder that the imagery resources are downloaded too, and extract all the required metadata from the files to utilise the imagery with Nechads universal turbidity equation.
This will only work with data downloaded from Planet Imagery.

Band number extracted: 1 (red)
Required inputs: path to imagery folder


#Remember to use double back slashes in your path!
#Note that time values are GMT+0, so should be treated accordingly

It will save the output in the same folder as the script as a csv file called 'metadata' - remember to rename and save this file as something else, otherwise it will be overwritten!

"""
#importing required modules
import xml.etree.ElementTree as ET
import os
import numpy as np
import datetime as dt
from pytz import timezone


#identifying and listing metadata xml files in a folder
path = 'C:\\410 Arcmap\\Imagery_batch1\\Dec14_Feb15_21_BuxtonTrc_psscene4band_analytic_sr_udm2\\files'
files = []
for filename in os.listdir(path):
	if filename.endswith('metadata_clip.xml'):
		files.append(filename)
	else:
		continue

#conversion of date and time data and adjusting for timezone difference
fmt = "%Y-%m-%d %H:%M:%S %Z%z"
def date_correct(date_norm, time_norm):
	date1 = date_norm + ' ' +time_norm
	date2 = dt.datetime.strptime(date1, "%Y-%m-%d %H:%M:%S")
	date_utc = date2.replace(tzinfo=timezone('UTC'))
	date_nz = date_utc.astimezone(timezone("Pacific/Auckland"))
	return(date_nz)
```

```
#creating blank data array and looping variables
data_collat = [[0 for i in range (len(files)+1)] for j in range(len(files)+1)]
data_collat[0] = ('Filename', 'Reflectance Coefficient', 'Band Harmonmisation', 'Offset', 'Date',
'Time', 'Cloud Cover', 'Unusable Data')
indexing_loop_val = 1

#looping through all identified metadata files in folder and extracting data
for current_file in files:
	current_file_path = path + '\\' + current_file.replace('\\','\\\\')
	#print(current_file)

	#parsing xml metadata file & navigation file
	tree = ET.parse(current_file_path)
	root  = tree.getroot()

	#pulling reflectance scale factor
	reflect_co = (root[4][0][5][2].text)

	#pulling band harmonisation factor
	try:
		band_co_array =  (root[4][0][5][3][3].text)
		band_co = band_co_array.split( )[0]
	except:
		band_co = 1

	#pulling final offset value
	try:
		offset =  (root[4][0][5][3][4].text)
	except:
		offset = 0

	#pulling date and time value and completing correction for timezone
	time_raw = (root[1][0][0].text)
	date = time_raw.split('T')[0]
	time = time_raw.split('T')[1]
	time = time[0:8]
	corrected = str(date_correct(date, time))
	date = corrected[0:10]
	time = corrected[11:19]

	#pulling unusable data mask and cloud cover
	cloud_cover = (root[4][0][2].text)
	#print(cloud_cover)
	unusable_mask = (root[4][0][4].text)
	#print(unusable_mask)

	#saving pulled values to data array and advancing indexing loop
```

```
data_collat[indexing_loop_val] = current_file, reflect_co, band_co, offset, date, time, cloud_cover, unusable_mask
          indexing_loop_val += 1

#Prints data, coverts to numpy array and saves as csv files
data_array = np.array(data_collat)
#print(data_collat)
np.savetxt('metadata.csv', data_array, delimiter=',', fmt='%s')
```